

OPTIMIZATION AND PERFORMANCE OF ADAPTIVE OPTICS FOR IMAGING EXTRASOLAR PLANETS

STEVEN M. STAHL¹ AND DAVID G. SANDLER^{1,2}

Received 1995 May 17; accepted 1995 September 11

ABSTRACT

A recent study by Angel (1994) using simplified analytical models indicated the feasibility of imaging extrasolar planets from the ground, making use of adaptive optics correction of a large telescope. We have performed detailed simulations of the method using computer codes that model propagation through atmospheric turbulence, adaptive correction, and broadband imaging. We confirm that high-resolution correction at the limit of photon noise errors reduces the halo intensity to 10^{-6} of the peak star flux. Our work shows how to avoid systematic errors. Thus, we find that time delays between sensing the wave front and its detection lead to persistent structure in the stellar halo, which uncorrected would prevent rapid averaging of the residual halo speckle structure. A local wave front reconstructor that extrapolates ahead in time has been devised to remove this problem. We find the chromatic differences in wave front structure are small enough that the signal-to-noise ratio can be improved by wave front sensing and imaging in separate adjacent bands. We verify that correction of amplitude scintillation is needed and the optimum level of clipping is derived. A simulated image of a twin of the solar system at 8 pc is presented for the new 6.5 m telescope and the measured turbulence at the Multiple Mirror Telescope site. The Jupiter twin shows up at the 5σ level in a 5 hr integration.

Subject headings: atmospheric effects — methods: observational — planets and satellites: general — turbulence

1. INTRODUCTION

Because of image blurring caused by turbulence in Earth's atmosphere, strategies to search for extrasolar planets have focused on indirect detection of stellar reaction motion (Black 1980). However, adaptive optics is rapidly emerging as a tool to produce diffraction-limited images for ground-based astronomical telescopes (Beckers 1993).

The adaptive optics method uses a deformable mirror (DM) to cancel phase aberrations by imposing an equal but opposite aberration before light is brought to a focus. Typically, pupil subapertures of size r_0 are used to measure and correct the wave front, where r_0 is the coherence length of the atmosphere, proportional to the size of the seeing disk and to $\lambda^{6/5}$, and λ is the imaging wavelength. To limit decorrelation caused by atmospheric winds, the interval between successive corrections is $\Delta t \sim t_0/2$, where $t_0 = 0.314r_0/v_w$ is the decorrelation time for atmospheric aberrations and v_w is an effective turbulence-weighted wind speed. For residual rms phase error $\sigma_\phi < 1$ rad, corresponding to near diffraction-limited performance, the Strehl ratio S for adaptive correction is approximately $\exp(-\sigma_\phi^2)$. In this regime, the corrected point-spread function (PSF) will consist of the Airy disk containing a fraction S of the energy, surrounded by a halo of speckled scattered light containing the fraction $1 - S$.

To achieve the extraordinary contrast ratio of $R = 10^9$ required to detect Jupiter-like planets, Angel's method relies on three factors:

1. Very strong reduction of the rms phase error and some reduction of the amplitude errors in the wave front. These reduce the fraction of the light scattered into a halo.

2. Complete decorrelation of the residual spatial errors over the range of scales corrected. This results in a broad, weak halo which is not centrally peaked.

3. A rapid correction cycle with complete decorrelation of temporal errors between cycles. This is needed if the halo noise in the integrated image is to average to the very low level required.

In the limit in which these goals are accomplished, we can formulate the capability to detect unresolved faint objects outside the Airy disk but within the isoplanatic patch in terms of the system gain G , defined as the ratio of the peak image intensity divided by the average halo intensity level. For a uniform halo, the gain is given by (Angel 1994) $G_{\text{unif}} = (1/\sigma_\phi)^2(D/d)^2$, where D is the telescope diameter and d is the width of pupil subapertures, which sets a lower limit on the scale of correction. The integration time T required for detection at contrast ratio R is given by

$$T = \tau(R \text{SNR}_p/G \text{SNR}_f)^2, \quad (1)$$

where τ is the exposure time required to obtain independent realizations of residual speckle in the halo, so that short exposures add according to the central limit theorem (Goodman 1985). The quantity SNR_p is the desired signal-to-noise ratio for the planet, and SNR_f is the SNR for a single short-exposure frame.

Angel showed it should be possible to achieve gain $G = 10^6$ for a 6.5 m telescope by operating at the theoretical performance limit ($\sigma_\phi = 0.15$ rad) imposed by photon noise errors in wave front sensing using light from the bright host star. Operating at this limit, with $\sim 10,000$ correction elements, direct detection is possible at contrast ratios of $R = 10^9$ in < 10 hr of integration.

To see if these goals can be accomplished in a practical adaptive system, we have performed the first simulations of high-resolution adaptive optics operating on a large telescope. We have incorporated realistic treatment of atmospheric scintillation, broadband speckle, speckle lifetime, chromatic effects, and Lyot stop (Lyot 1939) to suppress high-order Airy rings. Our approach differs in principle from schemes using lower order adaptive optics to detect exoplanets. Nakajima

¹ ThermoTrex Corporation, 9550 Distribution Avenue, San Diego, CA 92121; sstahl@cts.com, dsandler@cts.com.

² Also Center for Astronomical Adaptive Optics, Steward Observatory, University of Arizona.

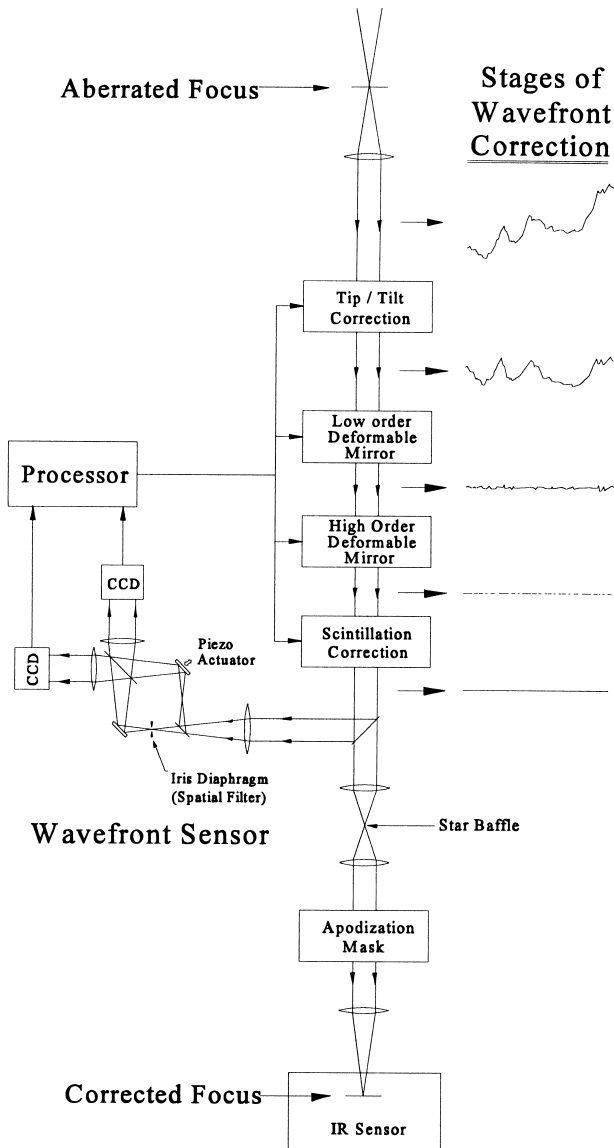


FIG. 1.—Schematic layout of adaptive optics system for exoplanet imaging.

(1994) studied very low order adaptive optics (30 correction elements) to narrow the PSF, with suppression of the stellar halo limited to that obtained by Lyot-type imaging optics. Labeyrie (1995) has recently proposed the use of adaptive correction operating at lower gain ($G \sim 10^4$) to infer the presence of a planet by using an array of photon-counting detectors to record dark spots (small regions of zero-photon events) that briefly appear in the image.

2. ADAPTIVE SYSTEM FOR EXTRASOLAR PLANET DETECTION

The correction of the wave front needed to suppress the stellar halo is made in four successive stages, as shown in Figure 1. After image motion correction, phase aberration is corrected in two stages, the first a conventional 300 actuator DM (Fugate et al. 1994) to remove the strongest, low spatial-frequency aberrations, followed by a high-resolution mirror to correct the residual fast-changing, fine-scale structure. Scintillation is then corrected by a fast liquid crystal (Bonaccini et al.

1991). Wave front phase and amplitude errors are measured using stellar light in a band from 0.65 to 0.9 μm by means of a Mach-Zehnder white-light interferometer (Angel 1994), operated in a closed-loop servo system. At the corrected focus, the star image is blocked by a small central stop, chosen to allow high imaging sensitivity at inner radii and to prevent interference with the halo. The surrounding field is relayed after pupil apodization to an infrared array, imaging in the 0.95–1.35 μm band.

Here we treat a $D = 6.5$ m telescope imaging a bright central star with flux 4×10^8 photons $\text{m}^{-2} \text{s}^{-1}$ in the wave front sensor wavelength band (R magnitude $m_R = 4$). Minimizing the residual mean-square error, we find $d = 5.5$ cm ($D/d = 118$) and $\Delta t = 0.5$ ms. The minimum wave front error at the mean imaging wavelength $\lambda = 1.15$ μm is $\sigma_\phi^2 = 0.03$ rad² (32 nm rms pathlength error), which in the uniform halo approximation corresponds to 3% of the energy in a broad halo of width $120 \lambda/D$. From equation (1), $G_{\text{unit}} = 0.4 \times 10^6$. We now discuss detailed simulations of the performance of the system of Figure 1, using these parameters.

3. SIMULATION METHOD

Atmospheric turbulence is represented by four Kolmogorov phase screens (Martin & Flatte 1990) corresponding to $r_0 = 0.4$ m at $\lambda = 1.15$ μm (0".7 seeing). The layer wind speed is 10 m s^{-1} for the lowest layer and 25 m s^{-1} for upper layers, giving $v_w = 15.6$ m s^{-1} and $t_0 = 8$ ms. The vertical profile is consistent with natural and laser guide star wave front data obtained at the Multiple Mirror Telescope (MMT) (Lloyd-Hart et al. 1995) and gives isoplanatic angle $\theta_0 = 8".2$ at $\lambda = 1.15$ μm and variance $\sigma_x^2 = 0.01$ of log-amplitude fluctuations (Goodman 1985).

A plane wave is propagated (Fleck, Morris, & Feit 1976) at 0.8 μm through the phase screens on a 512×512 grid with 360 points across the 6.5 m aperture ($r_0/8$ phase resolution). The Mach-Zehnder wave front sensor measurements are modeled as average phase values (pistons) over each square subaperture, and random Gaussian photon noise is added. The piston measurements are applied to a segmented adaptive mirror (Sandler et al. 1994) composed of $(\pi/4)(D/d)^2 = 11,400$ independent square segments each controlled in piston, tip, and tilt by piezoelectric transducer actuators. We compute each segment tip and tilt by differencing the pistons adjacent to the given segment. The measurement is then the local slope over width $2d$, which is taken as an estimate of the desired tilt over width d . The resulting fitting error is comparable to the fitting error for continuous DMs with single actuators separated by distance d (Angel 1994).

The intensity fluctuation data required for scintillation correction are provided by the pixel readouts of the Mach-Zehnder interferograms. To vary the degree of scintillation correction, we used an intensity mask that clips all pixel intensities values above a given threshold value. The optimum threshold was determined by numerical studies to be 0.64 times the average intensity across the pupil, which leads to a 40% loss of light into the imaging camera.

For each short exposure, monochromatic plane waves are propagated through the phase screens starting at a wavelength of 0.95 μm and increasing to 1.35 μm in increments of 0.025 μm . At each wavelength the field is passed through a Gaussian central stop of rms width 0".18. The beam is then expanded to a pupil, where Lyot-type edge apodization is carried out with

a pupil mask that smoothly reduces the light beyond diameter $0.9D$. An image at the detector for each wavelength is obtained by final fast Fourier transform, and a broadband image is obtained by incoherent superposition.

4. RESULTS FOR MINIMIZING THE STELLAR HALO AND SPECKLE NOISE

Halo profile and system gain.—A cross section of the PSF $P(\theta)$ for an average of 64 short exposures (32 ms) is given in Figure 2 (*top*), starting with the case of uncorrected turbulence and moving through successively higher degrees of wave front correction. Different curves are for different wave front computation algorithms and hardware. The first level of improvement is for phase correction only, with the correction signals for each point on the DM set equal to the most recently measured phase error at that point in the pupil. The effect of very high resolution, high-speed correction is an enormous reduction in the halo, with gain $G = 0.2 \times 10^6$ at $\theta = 0''.6$ (5 AU at 8 pc). The next level of improvement is obtained with amplitude correction. After correction of scintillation, the gain increases to $G = 0.4 \times 10^6$, which is fortuitously equal to G_{unif} . For $\theta > 1''$, the gain levels out at $G = 0.7 \times 10^6$.

There remains central peaking by a factor of 2. This shows the residual error is spatially correlated on a scale larger than the subaperture size. The reason is that the time derivative of the phase is spatially correlated and thus also is the error arising from a lag between phase measurement and imaging. We have explored filters to predict the temporal evolution on the basis of neighboring and previous measurements. The coefficients of the filter depend on the prevailing wind velocity v_w and are determined from minimum variance estimation procedures (Schwartz et al. 1994). For the turbulence used in the simulation, we find an optimized local spatial filter of the form $p_i(t + \Delta t) = \sum w_{ij} p_j(t)$, where the sum includes actuator i and its eight nearest neighbors. Use of the filter reduces the mean square temporal error by a factor of 5, thereby enhancing the gain to $G = 1.1 \times 10^6$, a factor of 2.6 increase over G_{unif} , which (eq. [1]) leads to a dramatic decrease in required integration time.

We note that after implementation of filtering, for $\theta < 1''$, $P(\theta)$ is an increasing function of θ , arising from a doughnut-shaped coherent halo due to periodicity in the tip-tilt error. Because the segment tilts are derived from adjacent piston measurements, neighboring tilt estimates share a common internal piston value, inducing strong correlations of period $\lambda/2d$. Thus, the doughnut has a broad maximum at $\lambda/2d = 2''$, as observed in the bottom curve of Figure 2 (*top*).

Halo fluctuation and smoothing with time.—The rms fluctuation due to speckle structure in a single exposure is about 0.36 of the mean value. We have used the sequences of 64 successively corrected images to investigate how well long exposures will improve the SNR, as illustrated in Figure 2 (*bottom*), which shows direct plots of the intensity on a circle of radius $0''.6$. The pixel values have been plotted as a function of angle around the circle. If there is complete decorrelation between successive frames, the noise reduction should be as the square root of the number of correction intervals. In practice, the simpler wave front solutions have strong temporal correlation and fall far short. This can be seen from the first two plots of Figure 2 (*bottom*). The uppermost is a single short exposure for phase correction only, while immediately below is the same case for an average of 64 frames. The integrated image for this case shows only a factor of 2 improvement,

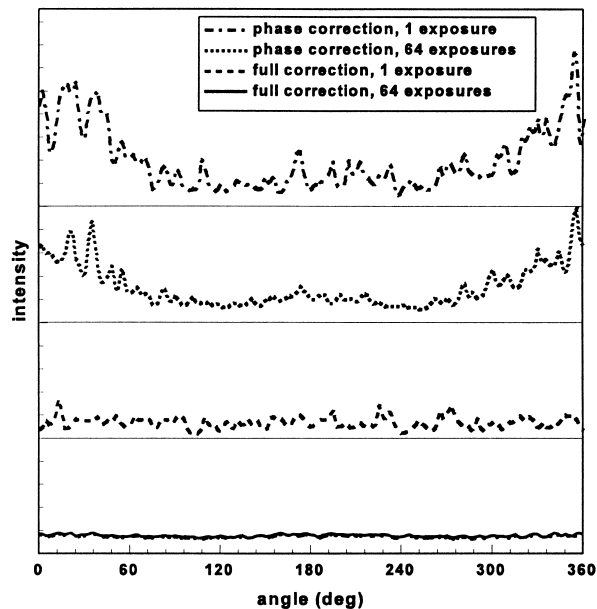
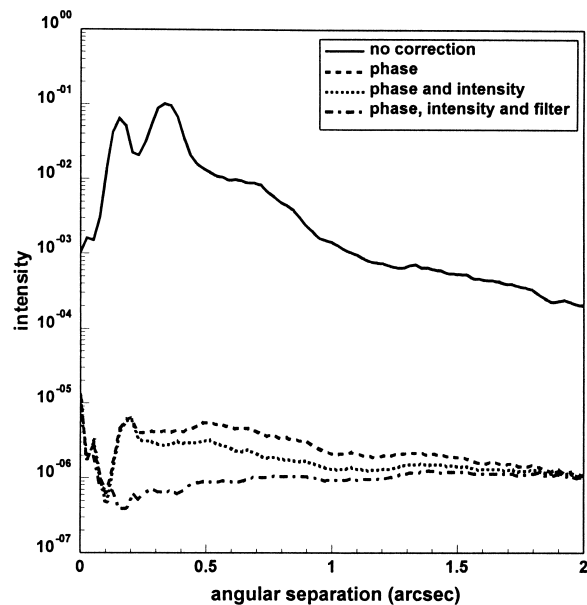


FIG. 2.—*Top*: slices of PSF for an average of 64 short exposures, illustrating the reduction in halo achieved by successively higher degree of correction. The intensity is normalized so that the on-axis peak would be unity for a stellar image without central stop. *Bottom*: plots of the intensity around a circle of radius $0''.6$, illustrating the reduction in fluctuations about the mean halo achieved by averaging and temporal filtering. *Top to bottom*: phase correction only, 0.5 ms short exposure; phase correction only, 32 ms exposure; phase and amplitude correction with local filtering, 0.5 ms exposure; phase and amplitude correction with local filtering, 32 ms exposure.

compared to the ideal factor of 8. This illustrates that residual low-frequency temporal errors lead to correlations in the short-exposure PSFs that persist for many frames. Note that the angular dependence of the speckle intensity plotted on a linear scale results from lag errors, since the error is strongest along the direction of the wind.

With appropriate corrective measures, the degrading effect of temporal correlations can be effectively eliminated. Scintillation effects, which give correlation over several milliseconds, are partially to blame, and, with these corrected, the improvement from averaging is a factor of 3. Finally, with filtering of wave front data, already prescribed to reduce spatial correlations, the fluctuation in the 64 frame integration drops by a factor of 7, which indicates that successive frames are nearly uncorrelated. Thus, the filter has also reduced temporal correlations. This can be seen from the bottom two plots of Figure 2 (*bottom*), which show intensity versus angle at 0".6 radius obtained using the wave front filter for both a single short exposure and for an average of 64. In using local filtering to suppress small-angle scattering from time delay errors, frame-to-frame correlations become small enough to approach the limiting dependence of T on SNR_r (eq. [1]). We note that the above conclusions were also supported by additional samples of 64 frames, using a different initial set of random phase screens.

5. CONCLUSIONS

These studies bring out the vital importance of designing a system that corrects for the spatial and temporal correlations from scintillation and time lag. Their combined effect in improving the gain and the effectiveness of temporal averaging results in a factor >20 in the SNR of an integrated image, corresponding to a factor >400 in integration time T . Thus, the feasibility of a survey of Jupiter-like planets around nearby stars hinges on adequately correcting amplitude and time lag errors.

A single short-exposure simulated image for the full correction method is shown in Figure 3*a* (Plate L22). We have simulated a long-exposure stellar image by extrapolating the 64 frame average using the halo and frame statistics described above and adding Poisson image noise. For a 5 hr exposure, a smooth halo is achieved for separations $>0".2$. The planet signal is simulated by computing the PSF of the system without a central stop. In Figure 3*b* we show a simulated 5 hr exposure of our solar system as seen from 8 pc. Jupiter stands out distinctly from the background, at $\text{SNR}_p = 5.5$.

Obviously, extreme control of all systematic errors will be needed to detect a signal at a level of 1/1000 of the background halo. Intensity spikes from stellar diffraction should not be a problem because of both radial smoothing arising from broadband imaging and rotation of the image during the 5 hr exposure. Small residual aberration in the uncompensated imaging path will produce a fixed speckle pattern, common to all bright reference stars, that must be very accurately characterized and removed.

In conclusion, we have shown that a new type of adaptive optics instrument with 11,000 correction segments controlled at a 2 kHz update rate is capable of detecting Jupiter-like planets orbiting nearby stars. Integration times practical for a survey of 30 bright stars within 10 pc can be achieved. The hardware requirements, while challenging, should be reachable in the near term. Segmented deformable mirrors have been developed and successfully tested over the past 10 yr (Hulburd & Sandler 1990) for both defense and astronomical applications. Mirrors of 500 segments have been built and demonstrated at ~ 10 nm accuracy at >2 kHz update rates, at strokes much larger than required for the high-resolution deformable mirror for exoplanet imaging, and the designs are scalable to the required 10,000 segments. A prototype of the direct phase sensing interferometer has been successfully tested at the Steward Observatory 2.3 m telescope (Colucci 1994). By moving one or both deformable mirrors out of a plane conjugate to the telescope pupil, it should be possible to control both phase and amplitude errors using the full set of phase and intensity measurements produced by the interferometer. Based on these considerations, a system design, scalable to the full exoplanet imaging system, is underway to perform proof-of-principle field tests at reduced aperture.

We thank J. R. P. Angel and Neville Woolf for numerous technical discussions and pointing the way to the possibility of imaging extrasolar planets from the ground. This work was supported by grant F49620-94-1-0437 from the Air Force Office of Scientific Research to the Center for Astronomical Adaptive Optics at Steward Observatory.

REFERENCES

- Angel, J. R. P. 1994, *Nature*, 368, 203
 Beckers, J. M. 1993, *ARA&A*, 31, 13
 Black, D. C. 1980, *Space Sci. Rev.*, 25, 35
 Bonaccini, D., et al. 1991, *Proc. SPIE*, 1534, 133
 Colucci, D. 1994, Ph.D. thesis, Univ. of Arizona
 Fleck, J. A., Morris, J. R., & Feit, M. D. 1976, *Appl. Phys.*, 10, 129
 Fugate, R. Q., et al. 1994, *J. Opt. Soc. Am. A*, 11, 310
 Goodman, J. W. 1985, *Statistical Optics* (New York: John Wiley and Sons)
 Hulburd, B., & Sandler, D. 1990, *Opt. Eng.*, 29, 1186
 Labeyrie, A. 1995, *A&A*, 298, 544
 Lloyd-Hart, M., et al. 1995, *ApJ*, 439, 455
 Lyot, B. 1939, *MNRAS*, 99, 580
 Martin, J. M., & Flatte, S. M. 1990, *J. Opt. Soc. Am. A*, 7(5), 838
 Nakajima, T. 1994, *ApJ*, 425, 348
 Sandler, D. G., et al. 1994, *J. Opt. Soc. Am. A*, 11(2), 858
 Schwartz, C., Baum, G., Ribak, E. N., & Lipson, S. G. 1994, *Proc. SPIE*, 2201, 180

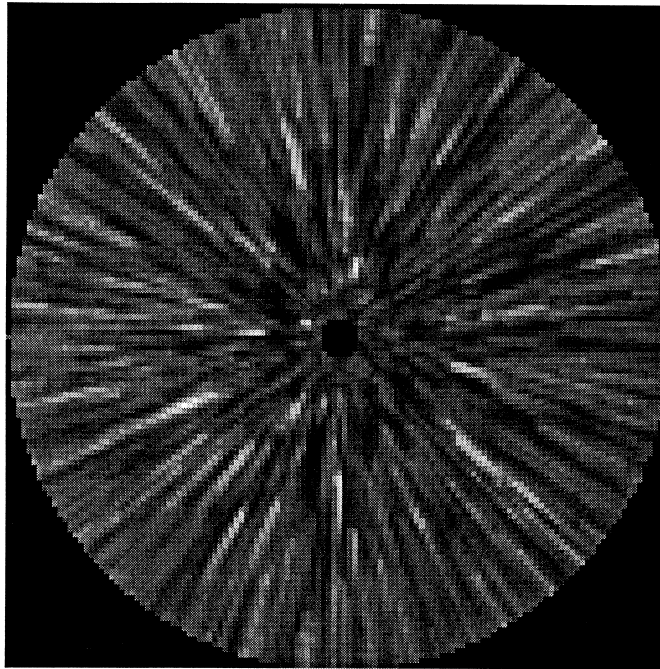


Figure 3a

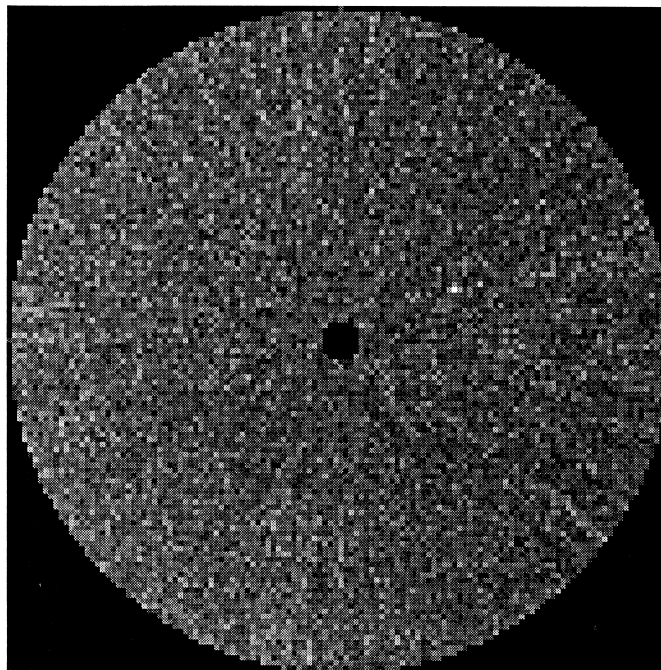


Figure 3b

FIG. 3.—(a) Simulated 0.5 ms exposure, corresponding to correction of phase, amplitude, and time lag errors. Photon noise has been omitted to show the speckle structure (due to residual adaptive optics errors) that must be averaged in long exposures to create a uniform halo. (b) Simulated 5 hr exposure of a solar system twin at 8 pc. Jupiter stands out at 2 o'clock at 5σ above the noise. The plate scale is $0''.025 \text{ pixel}^{-1}$.